Decarburization during laser surface processing of steel

Niroj Maharjan[1, 2], Wei Zhou[1,*], Yu Zhou[2], Naien Wu[3]

[1]*School of Mechanical and Aerospace Engineering, Nanyang Technological University, 50 Nanyang Avenue, Singapore 639798*

[2]*Advanced Remanufacturing and Technology Centre, 3 CleanTech Loop, Singapore 637143*

[3]*Precision Laser Solutions Pte. Ltd, 280 Woodlands Industrial Park E5, Singapore 757322*

* Corresponding author

E-mail address: wzhou@cantab.net; *Tel:* +65 6790 4700

Abstract

Unwanted removal of carbon from surface may occur during laser surface processing of steels despite the short interaction time and thermal cycle. However, no attention is paid in literature to investigate this phenomenon systematically. This paper presents two different scenarios during laser surface processing of steels: complete absence of decarburization for an alloy steel but decarburization with depth up to 70 μm for a plain carbon steel, showing that alloying elements tend to retard decarburization process by reducing the mobility of carbon in austenite. Further analysis reveals that the laser induced decarburization is dependent primarily on peak temperature and austenitization kinetics.

Keywords: Decarburization, Laser surface processing, Steel, Hardness

1 Introduction

Decarburization is a well-known surface degradation process involving loss of near-surface carbon from steel during exposure in air at elevated temperatures [1]. As a result of near-surface carbon loss, the surface of the steel has a lower strength, lower fatigue resistance and higher wear rate [2]. The problem has been prevalent during high temperature heat treatments carried out in industrial operations such as rolling and forging.

Unlike in conventional heat treatment, laser surface treatment produces a rapid heating condition at the surface characterized by high heating kinetics and short austenitization periods [3]. Despite the short interaction time, there is a chance of carbon loss from the surface. Some studies have mentioned the possibility of decarburization after laser surface treatment as one of the reasons for degraded surface mechanical properties. Kwok et al. [4] found higher degree of decarburization at slow scanning speed during laser surface melting of stainless steel. Abboud et al. [5] predicted the possibility of decarburization even when annealing time is short during laser surface treatment of carbon steel; but failed to provide any details. Similarly, Yan and co-workers [6,7] reported a sharp decrease in surface hardness of plasma-nitrided and laser quenched steel specimens. They identified decarburization at high temperature produced by laser quenching as one of the reasons for such hardness reduction. Moreover, Zhao et al. [8] investigated decarburization during selective laser melting of stainless steel. They found 21% carbon loss during the process which resulted in low hardness and tensile strength. Although selective laser melting is not exactly a surface processing technique, their results indicate the possibility of carbon loss from the surface during laser surface processing. However, an elaborative investigation on quantifying the decarburization during laser surface treatment is still missing.

In this paper, we study the laser induced decarburization in steel surface both experimentally and analytically. A comparison of laser induced decarburization with furnace heating is also presented. Moreover, the factors affecting decarburization kinetics during rapid laser heating are also discussed.

2 Experimental Procedure

2.1 Materials

AISI 1055 steel and 50CrMo4 steel were used for current study. The chemical composition and the as-received microstructure of these steels are shown in Table 1 and Fig. 1 respectively. AISI 1055 steel is a medium carbon steel with initial microstructure consisting of ferrite and pearlite. 50CrMo4 steel is a low alloy bearing steel with spherical and elongated carbides in ferritic-pearlitic matrix. Both AISI 1055 and 50CrMo4 steels were obtained as cylindrical bars of 100 mm and 130 mm diameter respectively. Specimens of 50 × 20 × 6 mm^3 dimensions were extracted from the mid-radius of the cylindrical bar for further studies.

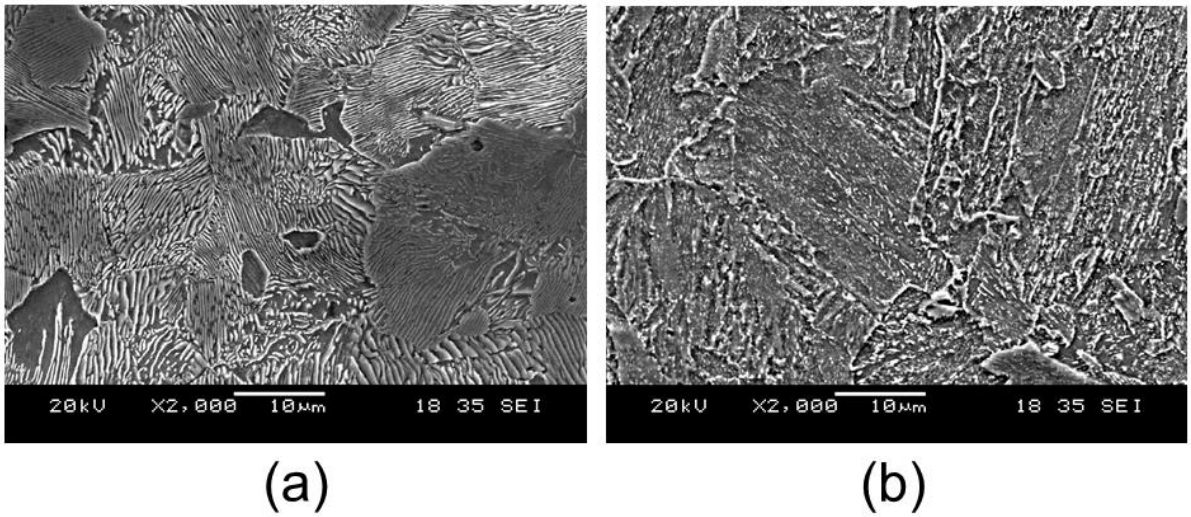

Fig. 1 As-received microstructures of **a** AISI 1055 steel showing ferrite and pearlite, and **b** 50CrMo4 steel showing elongated carbides in ferritic matrix

Table 1 Chemical composition (in wt%) of steels used

	C	Cr	Mn	Mo	Si	P	S	Ni	Cu	B	Fe
AISI 1055	0.56	0.11	0.78	-	0.23	0.01	0.002	0.07	0.06	0.0015	Bal.
50CrMo4	0.51	0.95	0.88	0.20	0.23	0.04	0.04	-	-	-	Bal.

2.2 Laser processing

Laser treatment was performed in a polished specimen using YLR-150/1500-QCW fiber laser (IPG Photonics) with a nominal power of 250 W. It produces a continuous wave laser beam of wavelength 1.07 μm. The laser beam was delivered to the work surface by focusing the beam through a lens of 300 mm focal length. A defocus distance of about 10 mm was maintained that produced a spot size of 0.5 mm at the surface and all experiments were carried out in air. A series of laser scans were performed to determine the best parameters for surface treatment. Based on the surface morphology and depth of hardening obtained, an optimized power density of 1.27×10^5 W/cm^2 with scanning speed of 10 mm/s was used.

In order to benchmark the decarburization in the steels, they were heat treated in a box furnace at 860°C for 20 minutes and cooled in open air. The total decarburization depth, which is defined as the distance from the surface to a location where the bulk carbon (hardness) is reached, was measured by micro-etching as well as by hardness measurement as stated in ASTM E1077-14 [9].

2.3 Characterization

After treatments, the cross sections were mechanically ground and polished using standard metallographic sample preparation technique. A 0.04 μm colloidal silica suspension was used for the final preparation step and the specimen was etched with a 2% Nital solution (2 ml HNO_3, 98 ml ethanol) for imaging with light optical microscopy (Carl Zeiss AxioCAM) and secondary electrons (JOEL 5600 LV SEM).

Microhardness measurements were made on the cross sections using Vickers hardness indenter at 100 gf and 15 s dwell time. As for the laser treated specimens, nanoindentation test was used instead of Vickers microhardness test since the laser hardened area was in the range of few hundreds of microns. Nanoindents were made using Agilent G200 nanoindenter with a Berkovich indenter. A surface approach velocity of 10 nm/s and a constant depth limit of 2000 nm was used to create a series of indents on the laser treated

surface. The average hardness for each point was measured using a depth range of 1000 to 1800 nm where the hardness values were more stable.

Both Vickers and Berkovich tips produce approximately 8% strain in the material during indentation; thus enabling direct comparison of the values [10]. However, it is noteworthy to point out that the hardness obtained from nano-indentation are generally 1.3-1.5 times higher than the hardness obtained from Vickers microindentation test. This can be ascribed to the size effect and the difference in contact area definition [11]. Nevertheless, since the main objective of using nanoindents in this study was to obtain a higher depth resolution in order to quantify decarburization, the difference has been ignored.

To evaluate the wear performance, dry friction wear tests of as-received and laser treated surfaces were performed on a ball-on-disk CETR UMT-3MT tribometer with a load of 10 N and a rotating speed of 240 rpm. A 3/8 inch 100Cr6 steel ball was used to roll on the surface creating a diameter of 5 mm on the surface. After every one hour interval of the test, the specimen was cleaned and weighed on precise mass measuring machine to calculate the mass removal by wear.

3 Results and Discussion

3.1 Furnace heating

Cross section metallographic studies were performed to analyze the extent of decarburization after furnace heating. Figure 2 shows the micrographs near the surface. In both steels, a thin white layer existed near the surface which was identified as ferrite. The formation of ferrite layer indicates the removal of carbon from the surface. Microhardness measurements were also made along the cross section to verify the loss of carbon. The results are shown in Fig. 3 which shows the reduction in hardness of the near surface layer due to decarburization. The decarburized layer was approximately 80 μm and 220 μm for 50CrMo4 and AISI 1055 steel respectively.

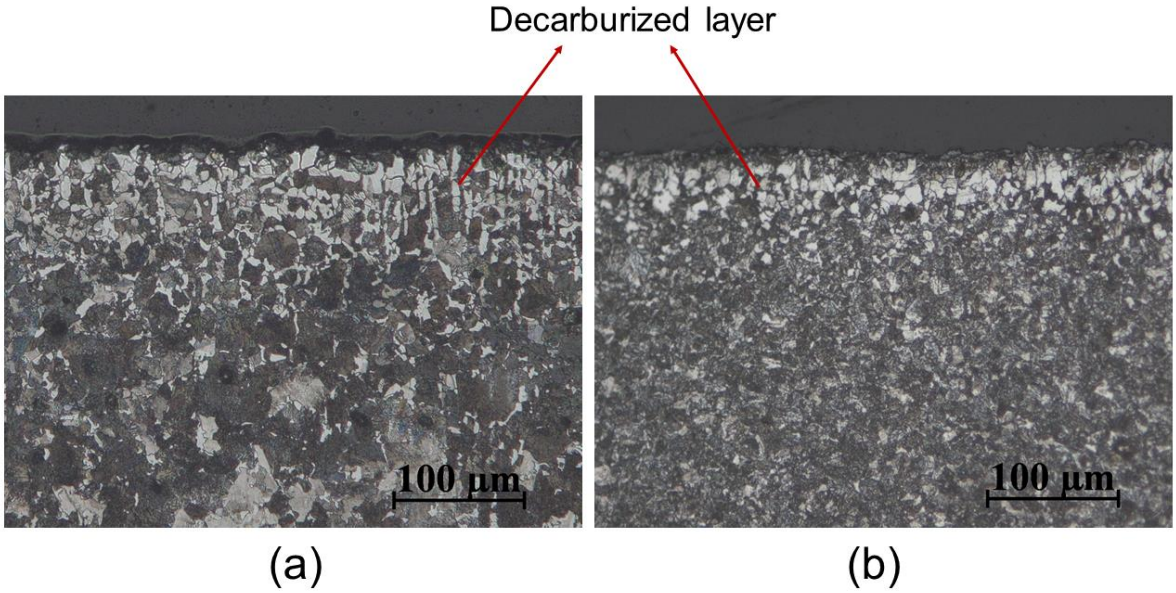

Fig. 2 Decarburized surface layers of **a** AISI 1055 steel, and **b** 50CrMo4 steel after the heat treatment in furnace

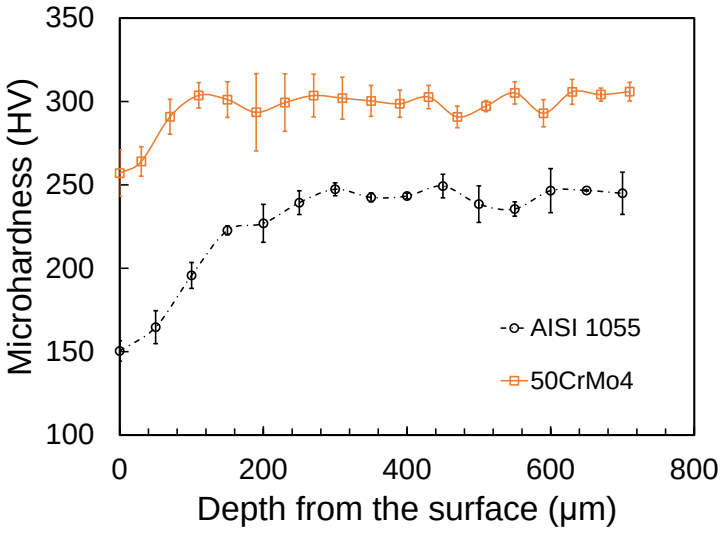

Fig. 3 Vickers microhardness profile showing decrease in surface hardness after the furnace heat treatment

3.2 Laser treatment

Laser surface processing produced a distinct microstructural transformation in both steels. Figure 4a shows the micrograph of a typical laser surface treated 50CrMo4 steel. The laser affected area can be clearly distinguished from the base microstructure from the optical micrograph. The microstructure predominantly consisted of plate martensite with some spherical carbide particles finely dispersed in the matrix (Fig. 4c). These stable carbides ($(Fe,M)_3C$ with M= Cr, Mo, Mn) were partially dissolved in the austenitic matrix due to rapid heating and cooling [12]. The laser surface processing of AISI 1055 also produced similar microstructural transformation (Fig. 4b). However, the difference in martensite morphology could be clearly appreciated. The cementite lamellae present in the original as-received microstructure was completed dissolved and it formed lath martensite near the surface as shown in Fig. 4d.

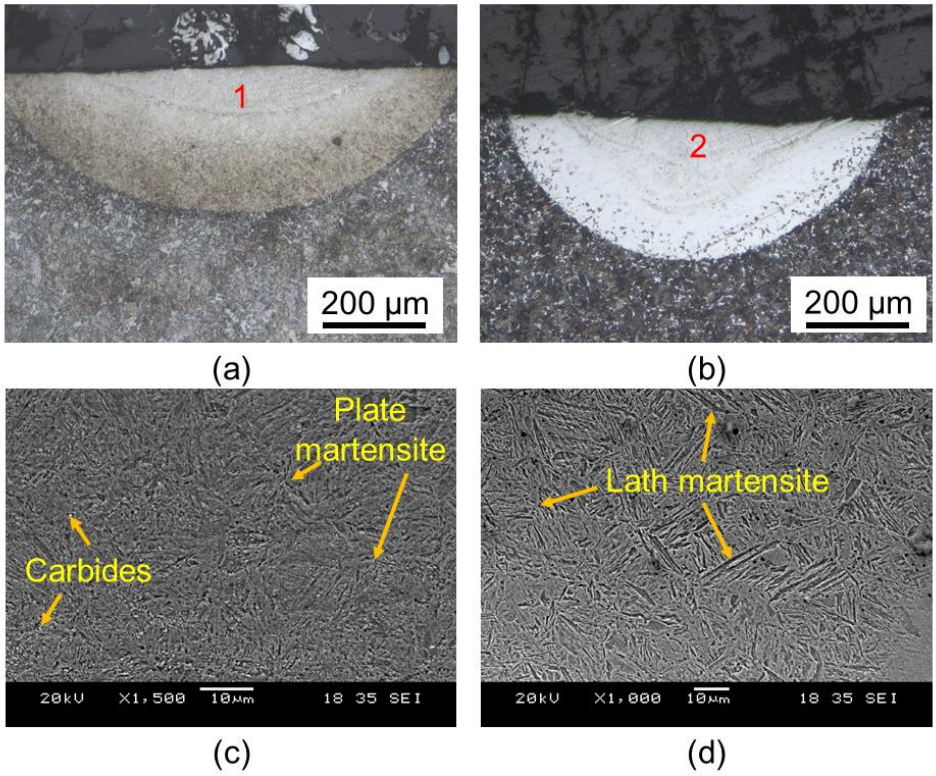

Fig. 4 Micrographs showing laser treated region of 50CrMo4 steel (a,c) and AISI 1055 steel (b,d) – **a,b** OM images showing overall laser affected region, and **c,d** SEM images showing higher magnification of region marked as “1” and “2” in a and b respectively

Since the laser treatment of steel is a rapid non-equilibrium process, decarburization during laser processing is not as obvious as in furnace heating. The laser heating quickly rises the surface temperature of steel above the austenitization temperature [3]. As the laser beam moves away, the heat energy quickly dissipates into the bulk substrate. This produces rapid cooling of the laser heated region resulting in non-equilibrium phase transformation in the austenitized region [13]. The rapid phase transformation forms martensitic structure as shown in Fig. 4c and 4d. The volume fraction and properties of martensite formed depends on the operating parameters and the material properties [14]. When in contact with decarburizing atmosphere such as air, the high temperature reached during laser processing provides enough energy for carbon to escape from the steel surface by reaction with atmospheric gases.

Microstructural analysis was thus carried out to investigate the possibility of decarburization during laser processing. However, it is very difficult to distinguish carbon loss from the surface just by using metallography as in furnace heat treated specimens [15]. This is due to the martensitic transformation which makes it difficult to characterize decarburization using optical micrography. Accurate measurement of chemical composition can help in analyzing the loss of carbon. To this end, energy dispersive spectrometry (EDS) was used to measure the carbon distribution. However, it did not reveal any difference probably due to large background noise intensity, atomic number effect (energy loss due to inelastic scattering) and absorption of X-rays [16]. While advanced analytical techniques to measure exact carbon content in steel exist [17–19], there is always a risk of surface contamination with adventitious carbon due to external exposure or handling of the specimen. This can lead to wrong interpretation of the results.

On the other hand, the measurement of hardness can be a good indicator of carbon removal from surface during laser treatment [20]. Hardness of martensite in steel is directly related to its carbon content [21]. Therefore, hardness measurements were made on the transverse section of laser treated surfaces. Owing to the limited depth affected by laser processing, a Berkovich nanoindenter was used to measure the hardness change near the surface. Figure 5 shows the hardness profile along the depth for the two steels studied. As expected, a very high hardness was obtained in the laser hardened region

compared to base microstructure for both steels due to phase transformation. No decrease in hardness near the surface was recorded for 50CrMo4 steel. Interestingly, AISI 1055 steel showed a slight decrease in hardness near the surface up to a depth of about 70 μm. This suggests possible loss of carbon from near surface region for AISI 1055 steel.

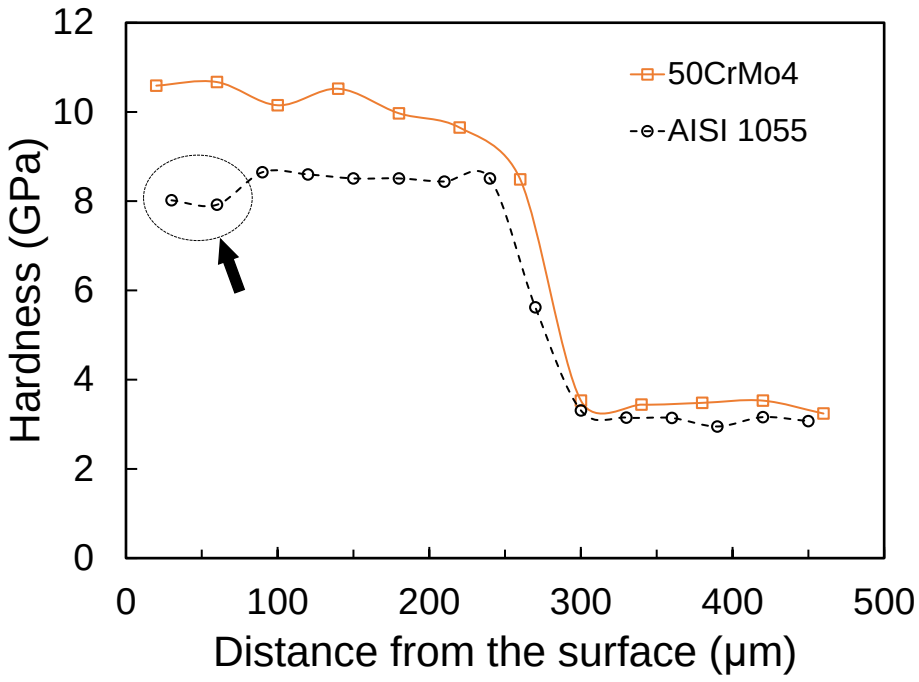

Fig. 5 Berkovich hardness profile after laser processing showing hardened surfaces for both steels but slightly lower hardness values (arrowed) for the top 100 μm surface layer of AISI 1055 steel

Decrease in hardness near the surface could arise due to other reasons as well such as grain coarsening [22] and formation of low hardened microstructure due to slow quenching rate [23]. However, the fact that the highest hardness occurred in the sub-surface region eliminates these possibilities. Furthermore, the SEM micrograph revealed presence of lath martensite in the near surface region of AISI 1055 steel as shown in Fig. 4d. Lath martensite occurs in a fully hardened microstructure of steels with low carbon content [21]. Therefore, this also verifies the loss of carbon near the surface during laser surface processing.

Compared to AISI 1055, the hardness profile for 50CrMo4 steel did not show any near-surface decrease in hardness (see Fig. 5) suggesting negligible decarburization in this steel. This can be attributed to the chemical composition and initial microstructure of the steels. Austenite formation kinetics has a substantial effect on mobility of carbon and hence, also dictates decarburization kinetics [24]. Austenitization of fine pearlitic microstructure (as in AISI 1055 steel shown in Fig. 1a) occurs very rapidly owing to less time required for dissolution of pearlite, particularly at higher temperatures. Therefore, it results in higher decarburization depth.

In contrast, 50CrMo4 steel consists of ferrite-pearlitic microstructure with spherical and elongated carbides distributed randomly in the matrix (see Fig. 1b). The dissolution of these carbides requires longer austenitization time than pearlite due to their low surface area [25]. Furthermore, presence of alloying elements such as Cr, Mn and Mo tend to reduce the diffusivity of carbon in austenite [26,27]. Gegner et al. [28] suggests that substitutional alloying elements significantly change the bulk diffusion coefficient of carbon in austenite even at low concentrations. Therefore, the decarburization kinetics for 50CrMo4 steel is significantly retarded which does not manifest any decrease in surface hardness. The study thus, shows that decarburization is significantly affected by the initial microstructure and presence of alloying elements in steel.

3.3 Modelling

The experimental studies revealed that decarburization can occur during laser surface treatment. In order to understand the kinetics of the process, a simple modelling of AISI 1055 steel for the simulation of the process was carried out using DICTRA software package in ThermoCalc [29].

During laser surface treatment, the temperature at the surface can reach to a very high temperature well above austenitization temperature. At such high temperature, the carbon can diffuse in or out of the metal surface depending on the interaction time and atmospheric condition [21]. The carbon potential between the material and the atmosphere is the driving force during the process which results in reaction of steel with

oxygen or moisture in the atmosphere. Another factor is the rate at which carbon diffuses from the interior to the surface of the steel.

The most basic chemical reaction occurring during decarburization is

$$C + CO_{2(g)} \leftrightarrow 2CO_{(g)} \quad (1)$$

This reaction is reversible and the relationship between the gaseous components and the carbon in solution of austenite (steel at high temperature) is described by fundamental law of mass action. It defines an equilibrium constant K, which is given as

$$K = \frac{P_{CO}^2}{f_c * wt\%C * P_{CO_2}} \quad (2)$$

where, P_{CO} and P_{CO_2} are the partial pressures of CO and CO_2 respectively and f_c is the activity coefficient of carbon.

The equilibrium constant, K, is a function of temperature, T (expressed in Kelvin) and is given by

$$\log K = -\frac{8918}{T} + 9.1148 \quad (3)$$

Knowing the partial pressure of CO_2 and CO, the equilibrium weight percent of carbon on steel at the given processing temperature can be predicted by rearranging (2)

$$wt\%C = \frac{1}{Kf_c}\frac{P_{CO}^2}{P_{CO_2}} \quad (4)$$

If the partial pressure of CO exceeds the partial pressure required to maintain a given carbon content, the reaction in (1) goes from right to left causing surface carburization until a new equilibrium is reached. On the other hand, if the CO_2 partial pressure is high

relative to CO content, the surface will be decarburized i.e. the reaction proceeds from left to right.

Equation (4) also requires determination of activity coefficient f_c which is a function of temperature and the composition of austenite. According to Harvey [30], f_c for Fe-Si-C system can be calculated by using following equation:

$$\log f_c = \frac{2300}{T} - 2.24 + \frac{179 + 8.9\, wt\%Si}{T} wt\%C + \left(\frac{62.5}{T} + 0.041\right) wt\%Si \quad (5)$$

Therefore, (2) to (5) can be used to calculate the equilibrium weight percent of C in the steel surface during decarburization. Apart from (1), other reactions such as reaction of carbon with water vapor and iron oxides may also occur at the surface [31], given as

$$C_{(Fe)} + H_2O_{(g)} \leftrightarrow CO_{(g)} + H_{2(g)} \quad (6)$$

$$C_{(Fe)} + FeO \leftrightarrow Fe + CO_{(g)} \quad (7)$$

These are not considered in the analysis. It is to be noted that decarburization is a complex process and a much higher CO content than CO_2 content is required for carburizing.

The diffusion of carbon inside austenite is determined by Fick's second law of diffusion, expressed as

$$\frac{\delta c}{\delta t} = -\frac{\delta J}{\delta x} \quad (8)$$

where, J is the net flux of carbon diffusing from a higher concentration to a lower concentration region. From Fick's law of diffusion, J is given by

$$J = -D\frac{\delta c}{\delta x} \tag{9}$$

where, D is the diffusion coefficient and $\frac{\delta c}{\delta x}$ is the concentration gradient.

Equation (8) demonstrates the basic principle of diffusion involved in decarburization. The diffusion coefficient varies according to the concentration gradient of carbon and the temperature, both of which are rapidly changing during laser treatment. Therefore, the expression for flux can be expanded as

$$J = -\sum_{j=1}^{n} D_j \frac{\delta c_i}{\delta x} \tag{10}$$

Equation (10) was solved numerically using ThermCalc DICTRA software using a method developed by Andersson and Ågren [32]. The solution yields the carbon concentration profiles at every step of the simulation. A simple one-dimensional geometry was adopted for the modelling as shown in Fig. 6. It provides carbon loss along the depth direction only which is sufficient to understand the effect of decarburization. Moreover, the simplicity of one-dimensional geometry helps to clearly appreciate the phenomenon with little sacrifice of accuracy and avoid complex calculations.

The system was considered as a single phase austenite region initially containing nominal composition of AISI 1055 steel. The equilibrium carbon concentration at the surface was calculated using (2)-(5), which was used as boundary condition. Both furnace heat treatment and laser surface treatment were modelled. The conditions for simulation were selected to match the parameters used for the experiments in Sections 3.1 and 3.2. Temperature profile was generated based on the laser parameter used. A typical thermal profile as shown in Fig. 6 was used as an input for modelling of laser surface treatment.

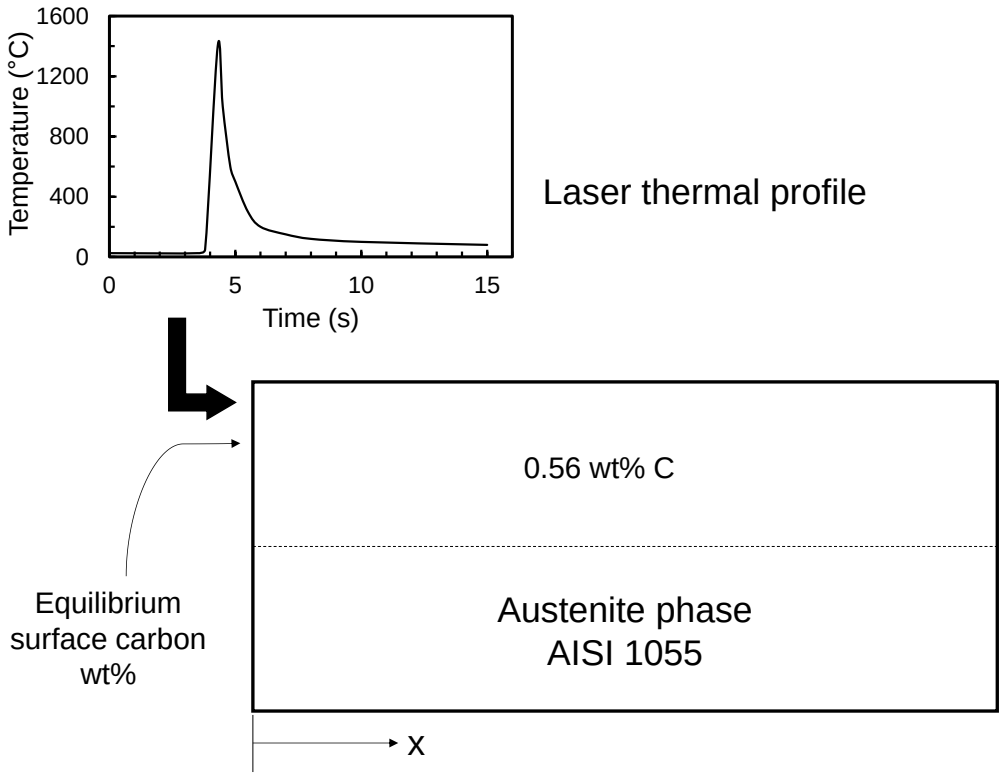

Fig. 6 Geometric scheme for modelling of decarburization during laser processing

Figure 7 shows the results of simulation as variation of carbon weight percent along the distance from the surface. In furnace heat treatment, the total decarburization depth was estimated to be about 300 μm (see Fig. 7a) which is close to the decarburization depth measured from optical micrograph and hardness measurements. The similar simulation and experimental results from furnace heating thus provided a benchmark and proved validity of the model.

As for the laser treated sample, the decarburization depth was very small compared to furnace heat treatment. Figure 7b shows the decarburization depth of about 65 μm for the laser conditions used in our experiment. The value is close to what was measured by nanoindentation test. It is noteworthy to point out that the equilibrium carbon weight percent at the surface for laser treatment was comparatively lower than that for furnace treatment. This is because of the higher peak surface temperature reached during laser

treatment. However, the short thermal cycle results in less decarburization depth than in furnace heating.

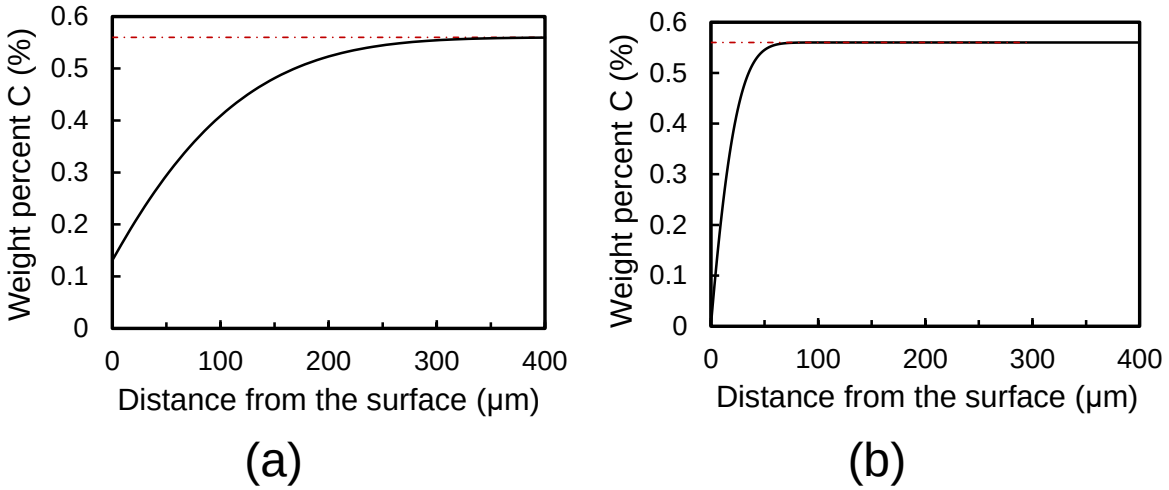

Fig. 7 Modelling results showing loss of carbon from the surface for **a** furnace heat treatment, and **b** laser surface treatment

The results exhibit the possibility of decarburization even during short thermal cycle induced by the laser beam. The loss of carbon is strongly dependent on the distance from the surface, as expected. The peak temperature reached during laser treatment, albeit for a short time, also has a big effect on decarburization depth as shown in Fig. 8. A very small decarburization depth is obtained for low peak temperature which increases exponentially with increase in peak temperature. However, the decarburization should not keep on increasing continuously as at higher temperature, the surface has higher chances of evaporation and ablation [33]. The modelling can serve as a powerful tool to predict the decarburization depth and/or optimize the process. Furthermore, the effects of various laser operating parameters on decarburization can be readily evaluated by simulation.

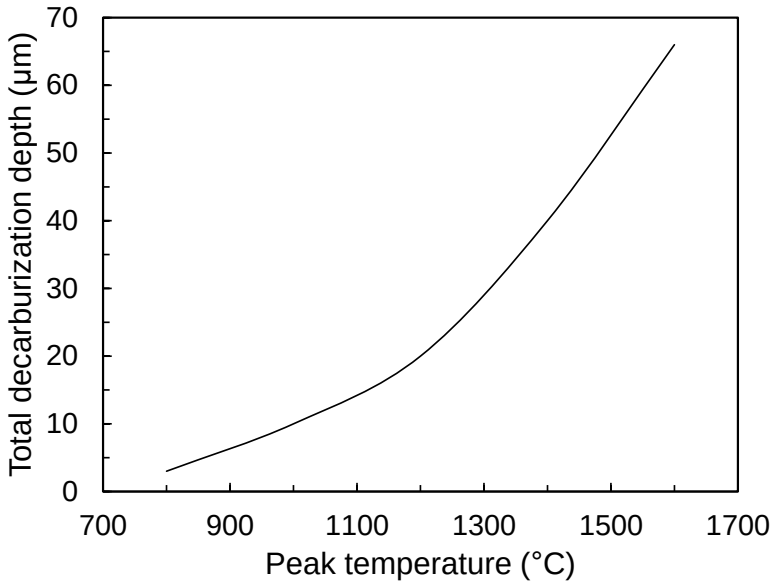

Fig. 8 Variation of decarburization depth with peak temperature during laser surface processing

3.4 Effect on practical performance

The laser surface treatment is generally performed to improve the surface mechanical properties of a component [34]. In order to evaluate the effect of decarburization on the practical performance of laser treated steel, dry friction wear tests were performed on as-received and laser-treated surfaces. Figure 9a compares the mass losses of laser treated and as-received substrate of AISI 1055 steel. As expected, an improved wear resistance was recorded for laser treated surface than as-received surface. The mass loss in laser treated specimen reduced by up to 54% compared to as-received material. The investigation of worn surface morphology revealed the presence of elongated scratch lines along the wear track of as-received surface due to its ductile nature (Fig. 9b). On the other hand, the laser treated surface had less deformed wear track due to the brittle nature of martensite (Fig. 9c).

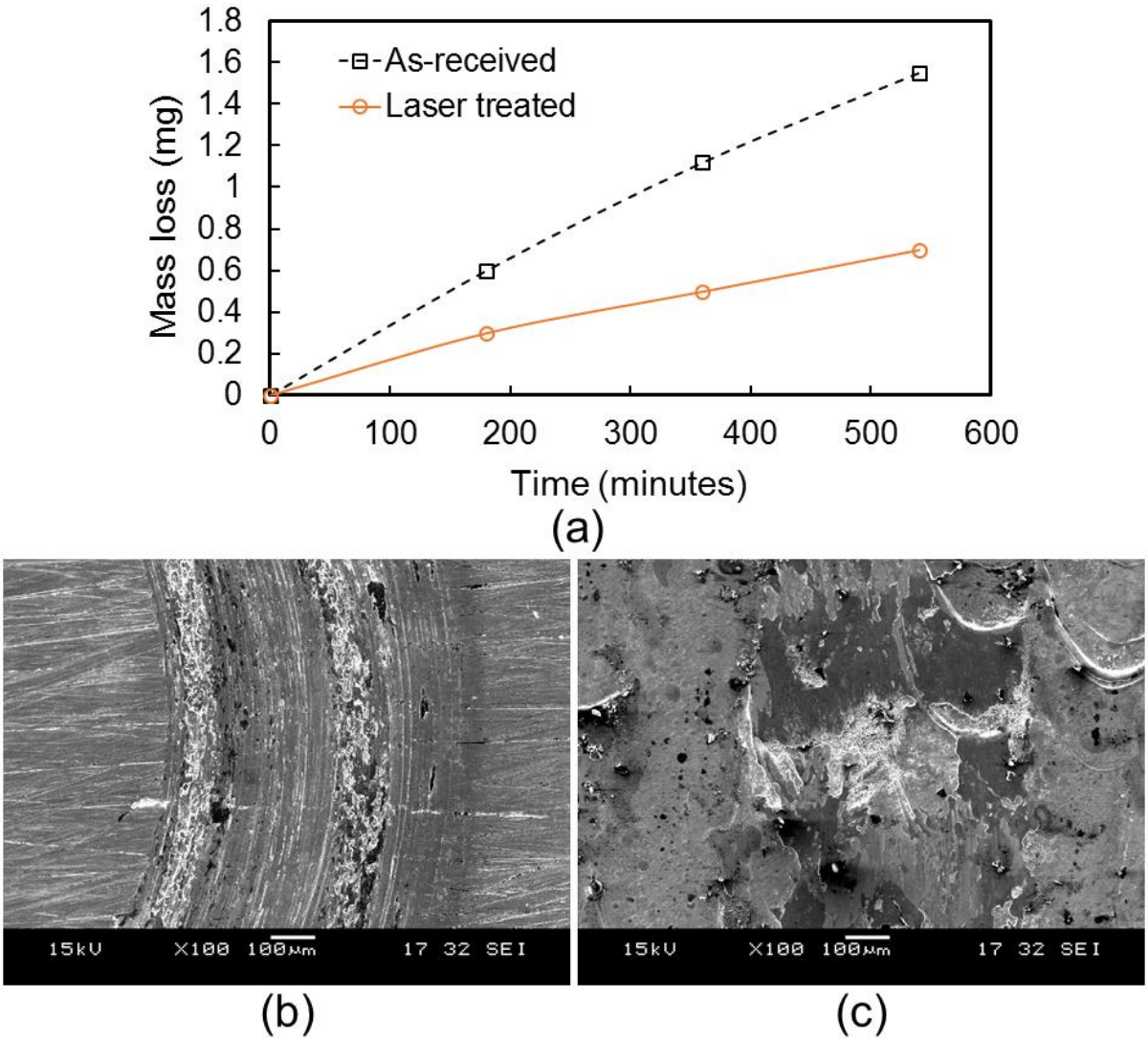

Fig. 9 Comparison of wear resistance of as-received and laser treated surfaces – **a** plot of mass loss against time, **b** wear morphology of as-received surface, and **c** wear morphology of laser treated surface

The improved resistance to wear is attributed to the rapid phase transformation during laser treatment [35,36]. In addition, significant improvements in corrosion resistance and high fatigue life have been reported in literature for laser treated surfaces [37,38]. Moreover, Kwok et al. [4] pointed out that mild decarburization during laser surface melting can be beneficial for corrosion resistance in stainless steel. Due to short interaction time and large temperature gradient, the carbon from the bulk do not get enough time to replenish the surface leaving more chromium in the solid solution of laser

treated specimen. This suggests that the detrimental effect of decarburization is suppressed by the rapid phase transformation brought about by the laser treatment. However, excessive decarburization always results in deterioration of the surface properties and should be avoided.

Having established the loss of carbon from surface during laser processing, it is imperative that certain actions be taken to prevent excessive loss of carbon from the surface. The most effective measure could be to prevent contact of steel surface with decarburizing atmosphere by using inert gas. However, it has been reported that mild decarburization can occur even in inert atmosphere [4]. Therefore, methods to counter the decarburization process such as coating with graphite or using some other carburizing medium during the process might be useful. This, not only helps to minimize decarburization, but can also be beneficial in increasing the surface properties of the material by influx of carbon. Further studies are being carried out in this direction.

4 Conclusion

In this investigation, decarburization of steel surface during laser treatment is evaluated both experimentally and analytically. It has been shown that decarburization can occur up to 70 μm below the surface of AISI 1055 steel despite fast kinetics of laser treatment. Even though the depth is approximately three times lower than in conventional furnace heat treatment, it shows that the heating during laser treatment austenitizes the surface providing ample condition for surface carbon to react with atmosphere and diffuse out. On the other hand, almost no carbon is lost from the surface for 50CrMo4 alloy steel. This is attributed to the presence of alloying elements which retards carbon mobility in austenite. Furthermore, the extent of decarburization is found to be primarily determined by the peak temperature reached during the process which is dependent on operating conditions of laser. Moreover, analysis of wear performance showed that the martensitic phase transformation due to laser treatment suppressed the detrimental effect of carbon loss from the surface and resulted in improved wear resistance compared to as-received surface.

Acknowledgements

Support from A*STAR SINGA Scholarship, Nanyang Technological University and Advanced Remanufacturing and Technology Center (ARTC), Singapore under the Collaborative Research Project RCA-15/287 is gratefully acknowledged.

References

1. D. Herring, *Atmosphere Heat Treatment: Atmospheres, Quenching, Testing - Volume 2*, 1st ed. (BNP Media, 2015).

2. R. I. Carroll and J. H. Beynon, Wear **260**, 523 (2006).

3. A. K. Nath and S. Sarkar, in *Adv. Laser Mater. Process. (Second Ed.* (Elsevier, 2018), pp. 257–298.

4. C. T. Kwok, K. H. Lo, F. T. Cheng, and H. C. Man, Surf. Coatings Technol. **166**, 221 (2003).

5. J. H. Abboud, K. Y. Benyounis, A. G. Olabi, and M. S. J. Hashmi, J. Mater. Process. Technol. **182**, 427 (2007).

6. M. F. Yan, Y. X. Wang, X. T. Chen, L. X. Guo, C. S. Zhang, Y. You, B. Bai, L. Chen, Z. Long, and R. W. Li, Mater. Des. **58**, 154 (2014).

7. Y. X. Wang, M. F. Yan, B. Li, L. X. Guo, C. S. Zhang, Y. X. Zhang, B. Bai, L. Chen, Z. Long, and R. W. Li, Opt. Laser Technol. **67**, 57 (2015).

8. X. Zhao, B. Song, Y. Zhang, X. Zhu, Q. Wei, and Y. Shi, Mater. Sci. Eng. A **647**, 58 (2015).

9. ASTM Subcomittee E04.14, 10 (2014).

10. P. L. Larsson, A. E. Giannakopoulos, E. Söderlund, D. J. Rowcliffe, and R. Vestergaard, Int. J. Solids Struct. **33**, 221 (1996).

11. L. Qian, M. Li, Z. Zhou, H. Yang, and X. Shi, Surf. Coatings Technol. **195**, 264 (2005).

12. T. Mioković, V. Schulze, O. Vöhringer, and D. Löhe, Acta Mater. **55**, 589 (2007).

13. S. N. Aqida, D. Brabazon, and S. Naher, Appl. Phys. A **110**, 673 (2013).

14. N. Maharjan, W. Zhou, Y. Zhou, and N. Wu, in *High-Power Laser Mater. Process. Appl. Diagnostics, Syst. VII* (International Society for Optics and Photonics, 2018).

15. A. Nagode, K. Jerina, I. Jerman, D. Vella, M. Bizjak, B. Kosec, B. Karpe, and B. Zorc, J. Sol-Gel Sci. Technol. **86**, 568 (2018).

16. J. I. Goldstein, D. E. Newbury, J. R. Michael, N. W. M. Ritchie, J. H. J. Scott, and D. C. Joy, *Scanning Electron Microscopy and X-Ray Microanalysis* (Springer, 2017).

17. Z.-Q. Liu, G. Miyamoto, Z.-G. Yang, and T. Furuhara, Acta Mater. **61**, 3120 (2013).

18. F. Boué-Bigne, Spectrochim. Acta Part B At. Spectrosc. **63**, 1122 (2008).

19. P. T. Pinard, A. Schwedt, A. Ramazani, U. Prahl, and S. Richter, Microsc. Microanal. **19**, 996 (2013).

20. G. F. Vander Voort, Adv. Mater. Process. 6 (2015).

21. G. Krauss, *Steels: Processing, Structure, and Performance* (ASM International, 2015).

22. E. Gharibshahiyan, A. H. Raouf, N. Parvin, and M. Rahimian, Mater. Des. **32**, 2042 (2011).

23. Z. X. Qiao, Y. C. Liu, L. M. Yu, and Z. M. Gao, Appl. Phys. A **95**, 917 (2009).

24. H. D. Alvarenga, T. Van De Putte, N. Van Steenberge, J. Sietsma, and H. Terryn, Metall. Mater. Trans. A **46**, 123 (2015).

25. H. Pantsar, J. Mater. Process. Technol. **189**, 435 (2007).

26. R. D. Cioffi and R. Wright, *A Comparison Study On Depth Of Decarburization And The Role Of Stable Carbide Forming Elements In 1075 Plain Carbon Steel And 440 A Stainless Steel* (New York, n.d.).

27. O. K. Rowan and R. D. Sisson, J. Phase Equilibria Diffus. **30**, 235 (2009).

28. J. Gegner, A. A. Vasilyev, P. J. Wilbrandt, and M. Kaffenberger, in *Proc. 7th Int. Conf. Math. Model. Comput. Simul. Mater. Technol.* (2012), p. 22.

29. J. O. Andersson, T. Helander, L. Höglund, P. Shi, and B. Sundman, Calphad **26**, 273 (2002).

30. F. J. Harvey, Metall. Mater. Trans. A **9**, 1507 (1978).

31. S. W. Mayott, *Analysis of the Effects of Reduced Oxygen Atmospheres on the Decarburization Depths of 300M Alloy Steel* (New York, 2010).

32. J. Andersson and J. Ågren, J. Appl. Phys. **72**, 1350 (1992).

33. N. Maharjan, W. Zhou, Y. Zhou, and Y. Guan, Appl. Phys. A **124**, 519 (2018).

34. W. Pakieła, T. Tanski, M. Pawlyta, K. Pakieła, Z. Brytan, and M. Sroka, Appl. Phys. A **124**, 263 (2018).

35. D. I. Pantelis, E. Bouyiouri, N. Kouloumbi, P. Vassiliou, and A. Koutsomichalis, Surf. Coatings Technol. **161**, 125 (2002).

36. C. P. Ma, Y. C. Guan, and W. Zhou, Opt. Lasers Eng. **93**, 171 (2017).

37. G. Telasang, J. D. Majumdar, G. Padmanabham, and I. Manna, Surf. Coatings Technol. **261**, 69 (2015).

38. S. Guarino, M. Barletta, and A. Afilal, J. Manuf. Process. **28**, 266 (2017).